Spins of complex fragments in binary reactions within a dinuclear system model

H. Paşca
Joint Institute for Nuclear Research, 141980 Dubna, Russia
and Department of Physics, "Babeş-Bolyai" University, 400084 Cluj-Napoca, Romania

Sh. A. Kalandarov and G. G. Adamian
Joint Institute for Nuclear Research, 141980 Dubna, Russia

N. V. Antonenko
Joint Institute for Nuclear Research, 141980 Dubna, Russia
and Mathematical Physics Department, Tomsk Polytechnic University, 634050 Tomsk, Russia
(Received 16 April 2017; revised manuscript received 6 September 2017; published 16 October 2017)

The average angular momenta and widths of the spin distributions of reaction products are calculated within the dinuclear system model. The thermal excitation of rotational bearing modes is considered in the dinuclear system. The calculated fragment spins (γ multiplicities) and their variances in the reactions ^{20}Ne (166 MeV) + ^{63}Cu, ^{40}Ar (280 MeV) + ^{58}Ni, ^{20}Ne (175 MeV) + ^{nat}Ag, ^{40}Ar (237 MeV) + ^{89}Y, ^{40}Ar (288 and 340 MeV) + ^{107,109}Ag, and ^{16}O (100 MeV) + ^{58}Ni are compared with the available experimental data. The influence of the entrance channel charge (mass) asymmetry and bombarding energy on the characteristics of spin distribution is studied.

DOI: 10.1103/PhysRevC.96.044611

I. INTRODUCTION

The dissipation of orbital angular momentum in fission and heavy-ion reactions has been the subject of experimental and theoretical interest for many years [1–30]. Of particular interest is the mechanism that converts the orbital angular momentum to the intrinsic fragment spins. In the classical picture, the two nuclei of the dinuclear system (DNS) are assumed to be rigid spheres rotating around a common center. As the nuclei interact through the long-range repulsive Coulomb forces and short-range attractive nuclear forces, the torques are generated upon the two nuclei causing their intrinsic rotation at the expense of relative angular momentum. If the condition of long interaction times is satisfied, the system attains equilibrium which corresponds to rigid rotation, characterized by matching the orbital and the intrinsic angular velocities. Then, the spin of the nucleus i after the DNS decay is defined by the following formula:

$$\langle I_i \rangle = \frac{\Im_i}{\Im_1 + \Im_2 + \Im_R} J, \tag{1}$$

where $\Im = \Im_1 + \Im_2 + \Im_R$ is the DNS moment of inertia in the sticking limit, $\Im_i$ is the moment of inertia of the DNS nucleus i [$i = 1 \equiv (Z_t - Z, A_t - A)$ or $2 \equiv (Z, A)$], $\Im_R = \mu R_m^2$ is the relative moment of inertia with the reduced mass parameter μ and the touching distance between the DNS nuclei, and J is the total angular momentum of the DNS with the total mass A_t and charge Z_t numbers. Because the nucleus-nucleus collisions occur with various impact parameters and, correspondingly, with various values of the orbital angular momentum, the use of the certain average value of J in Eq. (1) implies a serious physical limitation in the interpretation. Several values of "average orbital angular momentum" were proposed, ranging from $J_{max}/2$ to $J_{max}/\sqrt{\pi}$, $J_{max}/\sqrt{2}$ or even J_{max}, where J_{max} is the maximum angular momentum in a given reaction.

As experimentally established, the amount of angular momentum transferred to the fragments in a completely relaxed collision is approximately consistent with the formation and evolution of the DNS. In the experiment, the measurement of γ-ray multiplicities and alignment of the fragment spins provides insight to the process of angular momentum transfer. The relationship between the γ-ray multiplicity $M_\gamma(Z,A)$ and the average spin $\langle I_{Z,A} \rangle$ of nucleus (Z, A) is often given in the literature [17] as

$$\langle I_{Z,A} \rangle = 2[M_\gamma(Z,A) - a_\gamma], \tag{2}$$

where a_γ is a constant between 0 and 6 defining the number of statistical transitions which can be inferred from the γ spectrum and are weakly related to the collective spin. The heavy-ion collisions have proved that the rigid rotation limit is indeed achieved. Using the classical mechanic's rigid rotation formula (1), the spin of the fission fragments can only be approximately reproduced for the symmetric fragmentations, and even this implies a "fitting" of the average orbital angular momentum J. However, the angular momenta of fission fragments determined by γ-ray measurements is usually lower at large asymmetries than those predicted by Eq. (1). Also, the experimental data for heavy targets and projectiles revealed that the sum of the spins of final fragments has a weak dependence on mass asymmetry, opposite to the classical picture. Several models have been proposed in order to explain the experimental angular momentum data: (1) the diffusion model [14,17,21] in which transport equations have been invoked and the time evolution of the DNS is explicitly treated and (2) the statistical model [8,9,17] in which the angular momenta associated with several collective rotational modes (two wriggling modes, two bending modes, one tilting mode, and one twisting mode) are investigated. The latter model leads to some overestimation of the average values of the fragment

spins, but provides an important insight on the origin and magnitude of the spin fluctuations around the average value.

The angular momentum plays an important role in the capture and quasifission (fully damped) processes, the formation of complex fragments and compound nucleus (CN), and the competition of decay channels in the excited CN [17,31–33]. The nuclear reaction mechanism at low bombarding energies is assumed to be determined rather uniquely by the impact parameter or the angular momentum. As shown in Ref. [34], high angular momentum favors the emission of high-energy α particles and the emission probabilities of charged particles increase with angular momentum. The experimental evidence of the strong effect of angular momentum on the charge distribution of complex fragments ($Z > 3$) has been revealed in Ref. [35]. Within the DNS model [32,33,36–38] the reaction mechanism [the fusion followed by binary decay or quasifission (fully damped process without the formation of CN)] is mostly determined by the angular momentum deposited in the system. Knowledge about the angular momentum dependence of the probability of complex fragment emission is very important for the production of exotic nuclei via cluster decay of CN [39–43].

The aim of the present work is to study the average angular momenta and widths of the spin distributions of binary reaction products within the DNS model [32,33,36,37]. For this purpose, the DNS is coupled with the modes bearing angular momentum [9]. In the DNS model, the complex fragment formation and decay is treated under the assumption that the primary fragments are produced by the collective motion of the DNS in charge asymmetry coordinate with further thermal escape over the Coulomb barrier. The DNS model has an advantage that both fusion-fission and quasifission processes are taken into account naturally. The dynamics plays a role at high angular momenta when the quasifission becomes important. The main ingredient of the DNS description is the sophisticated potential energy (driving potential) as a function of angular momentum. The emission barriers for complex fragments are calculated within the DNS model by using the double-folding potential (with the Skyrme-type density-depending effective nucleon-nucleon interaction) for the nuclear part of the nucleus-nucleus interaction potential. Both the evaporation and binary decay are treated in the same way. In comparison with the statistical model [44,45], the definition of the emission barriers is more accurate in our case. In the DNS model, $J_{\max}$ is not an adjustable parameter, but it is calculated by using the nucleus-nucleus interaction potential [36]. The scission configuration is exactly defined and the temperature is precisely calculated for each fragmentation. The exact calculations of the temperature and angular momentum fractionation [8,17] (because the driving potential depends on the angular momentum) allow us to follow the evolution of the twisting, tilting, and bending modes in more detail, and to assess their contributions in the fragment spins with changing different experimentally controllable parameters. Note that in the works done in the eighties, the temperature seemed to be an adjustable parameter and the same for all fragmentations. Note that within the DNS model the charge, mass, and isotopic distributions of the products in the fusion-fission and quasifission reactions have been successfully described [32,33,36,37].

The results of the present paper are summarized as (a) a simultaneous treatment of the mass, charge, and spin distributions in the fusion-fission and quasifission reactions; (b) an explanation of the experimental data, especially at large mass and/or charge asymmetries; (c) a more detailed calculation of the variances arising from the orbital motion and bearing modes; (d) a saturation of intrinsic spin of fragments at a specific value of the bombarding energy; (e) a role of the angular momentum deposited into the system; and (f) a connection between the entrance channel and the spin of fragments. The model proposed is described in Sec. II. The detailed theoretical study of the reactions ^{40}Ar (280 MeV) + ^{58}Ni, ^{20}Ne (175 MeV) + ^{nat}Ag, ^{40}Ar (237 MeV) + ^{89}Y, ^{40}Ar(288, 340 MeV) + ^{nat}Ag, and ^{16}O (100 MeV) + ^{58}Ni is carried out in Sec. III. The conclusions are given in Sec. IV.

II. MODEL

A. Evolution in charge and mass asymmetries and decay in relative distance

The DNS model [32,33,36,37] describes an evolution of the charge and mass asymmetry degrees of freedom, which are defined here by the charge and mass (neutron) numbers Z and A ($N = A - Z$) of the light nucleus of the DNS, in the DNS formed in the entrance channel of the reaction after the dissipation of kinetic energy and angular momentum of relative motion. According to this description, there are nucleon drift and nucleon diffusion between the DNS nuclei and eventually either the CN is formed (complete fusion) or the DNS with given Z and A is formed and decays in the relative distance R between the centers of mass of the nuclei (quasifission). After the formation, the excited CN decays by various channels including the formation of certain DNS and their decay. The CN formation and its subsequent decay is not necessarily the ultimate result of the evolution of the initial DNS. In addition to contributions from the CN decay, the binary decay component is related to the quasifission mechanism. The competition between the complete fusion and quasifission depends on the value of the maximum angular momentum deposited in the system. The quasifission and CN decays are hardly distinguished in the experiments because in both cases two fragments are produced by the decay of the DNS formed during the diffusion process in the mass (charge) asymmetry coordinate with and without the stage of the CN formation.

The production cross section of nucleus with charge Z and mass A numbers is calculated as follows [32,33,36,37]:

$$\sigma_{Z,A}(E_{\rm c.m.}) = \sum_{J=0}^{J_{\max}} \sigma_{Z,A}(E_{\rm c.m.}, J) = \sum_{J=0}^{J_{\max}} \sigma_{\rm cap}(E_{\rm c.m.}, J) W_{Z,A}(E_{\rm c.m.}, J), \quad (3)$$

where $\sigma_{\rm cap}$ is the partial capture cross section which defines the transition of the colliding nuclei over the Coulomb barrier and the formation of the initial DNS when the kinetic energy $E_{\rm c.m.}$ above the barrier and angular momentum J of the relative motion are transformed into the excitation energy and angular momentum of the DNS. This transition

probability is calculated with the Hill-Wheeler formula, where the effective nucleus-nucleus potential V is approximated near the Coulomb barrier at $R = R_b$ by the inverted harmonic-oscillator potential. The maximum value of angular momentum $J_{\max}$ is limited by either the kinematical angular momentum $J_{\rm kin} = [2\mu(E_{\rm c.m.} - V_b)/\hbar^2]^{1/2} R_b$ (V_b is the height of the Coulomb barrier) or by the calculated critical angular momentum $J_{\rm cr}$ (at which the potential pocket of the nucleus-nucleus interaction potential disappears and the capture of projectile by the target becomes impossible) depending on which one is smaller: $J_{\max} = \min[J_{\rm kin}, J_{\rm cr}]$.

It should be noted that the calculated capture cross sections with this method are in a good agreement with those obtained with the dynamical model [46]. The value of

$$W_{Z,A}(E_{\rm c.m.}, J) = \frac{P_{Z,A} P^R_{Z,A}}{\sum_{Z',A'} P_{Z',A'} P^R_{Z',A'}} \tag{4}$$

is the formation-decay (emission) probability of the DNS with a given asymmetries Z and A. The probability

$$P_{Z,A}(E_{\rm c.m.}, J) \sim \exp[-U(R_m, Z, A, J)/T_{\max}(J)] \tag{5}$$

of the DNS formation is calculated statistically by using the stationary solution of the master equation with respect to the charge and mass asymmetries and depends on the potential energy $U(R_m, Z, A, J)$ of the DNS configurations at touching distance R_m and on the thermodynamical temperature $T_{\max}(J)$. The probability

$$P^R_{Z,A}(E_{\rm c.m.}, J) \sim \exp\left[-B^{qf}_R(Z, A, J)/T_{Z,A}(J)\right]. \tag{6}$$

of the DNS decay in the relative distance R is calculated by using the transition state method. This probability depends on the difference $B^{qf}_R(Z, A, J)$ between the potential energies of the DNS configurations at the touching distance and at the barrier position. The barrier B^{qf}_R, called quasifission barrier, prevents the DNS decay in R. In Eqs. (5) and (6), $T_{\max}(J) = \max\{T_{Z,A}(J)\}$, where $T_{Z,A}(J)$ are the temperatures of all possible configurations. These temperatures are calculated within the Fermi-gas model. The level density parameter a is taken as $a = 0.114A + 0.162A^{2/3}$ from Ref. [47]. The details of calculations of $\sigma_{\rm cap}$, $W_{Z,A}$, and, correspondingly, $\sigma_{Z,A}(E_{\rm c.m.})$ are given in Ref. [36]. Here, only the most salient features are outlined.

B. Spin of fragments from orbital momentum and bearing modes

The orbital motion of the system is not the only source of intrinsic spin of the fragments [17]. The collective angular oscillations (the bending, wriggling, tilting, and twisting modes) are also generated by thermal excitation of the DNS. Let us fix a reference frame with the y axis coinciding with the line of nuclear centers and the x and z axes perpendicular to it. The two bending modes correspond to a spin of one fragment parallel to the x or z axis associated with an opposite rotation of the other fragment. The twisting modes correspond to a rotation of one fragment around the y axis associated with an opposite rotation of the other fragment. The two wriggling modes are rotations of both fragments around the x or z axis compensated by a counter-rotation of the system as a whole about the same axis. Finally, the tilting mode describes the inclination angle of the total angular momentum with respect to the y axis. In general, because these collective modes are not exactly normal but are weakly coupled to the intrinsic modes, they can be thermally excited.

Thus, the collective angular modes as well as the rigid rotation (the orbital) mode contribute to the angular momenta and rotational energy of the fragments. In some instances, such as in γ-ray multiplicity measurements, we are interested in the average sum of moduli of the fragment spins from the different modes. Then, the average spin of the fragment (Z, A) is written as

$$\langle I_{Z,A}\rangle = \frac{\sum_{J=0}^{J_{\max}} I^T_{Z,A}(J)\sigma_{Z,A}(E_{\rm c.m.}, J)}{\sum_{J=0}^{J_{\max}} \sigma_{Z,A}(E_{\rm c.m.}, J)}, \tag{7}$$

where

$$\begin{aligned} I^T_{Z,A}(J) &= I^{\rm Rigid}_{Z,A}(J) + I^{\rm Bearing}_{Z,A}(J) \\ &= I^{\rm Rigid}_{Z,A}(J) + I^{Tw}_{Z,A}(J) + I^{Ti}_{Z,A}(J) + I^{B}_{Z,A}(J) + I^{W}_{Z,A}(J) \end{aligned} \tag{8}$$

is the sum of the pure orbital $I^{\rm Rigid}_i$, twisting I^{Tw}_i, tilting $I^{Ti}_{Z,A}$, bending I^B_i, and wriggling I^W_i spin components of the fragment [see Appendix A]. One can perform the averaging over all possible mass numbers A at fixed Z:

$$\langle I_Z\rangle = \frac{\sum_A \langle I_{Z,A}\rangle}{\sum_{Z,A}\langle I_{Z,A}\rangle}. \tag{9}$$

The large variance of the spin distribution of the fragments can be explained only by the contributions from the orbital and bearing modes. The total spin variance

$$\sigma^I_{Z,A} = \frac{\sum_{J=0}^{J_{\max}} \sigma^T_{Z,A}(J)\sigma_{Z,A}(E_{\rm c.m.}, J)}{\sum_{J=0}^{J_{\max}} \sigma_{Z,A}(E_{\rm c.m.}, J)} \tag{10}$$

originates from the variances of the rigid rotation and the bearing modes. Here,

$$\begin{aligned} \sigma^T_{Z,A}(J) &= \sigma^{\rm Rigid}_{Z,A}(J) + \sigma^{\rm Bearing}_{Z,A}(J) \\ &= \sigma^{\rm Rigid}_{Z,A}(J) + \sigma^{Tw}_{Z,A}(J) + \sigma^{Ti}_{Z,A}(J) \\ &\quad + \sigma^{B}_{Z,A}(J) + \sigma^{W}_{Z,A}(J) \end{aligned} \tag{11}$$

is the sum of orbital $\sigma^{\rm Rigid}_{Z,A}$, twisting $\sigma^{Tw}_{Z,A}$, tilting $\sigma^{Ti}_{Z,A}$, bending $\sigma^B_{Z,A}$, and wriggling $\sigma^W_{Z,A}$ variances [see Appendix A]. One can perform the averaging $\sigma^I_{Z,A}$ over all possible mass numbers at given Z:

$$\sigma^I_Z = \frac{\sum_A \sigma^I_{Z,A}}{\sum_{Z,A}\sigma^I_{Z,A}}. \tag{12}$$

In Ref. [9], the wriggling mode, consisting of the rotation of both fragments in the same direction (the light nucleus carries the bulk of the spin) and the rotation of the whole system in the opposite direction, is also described. Although this motion is possible in the classical description, the quantum mechanical calculations show that the energy required to activate this mode is much higher than the energy needed for the twisting, tilting,

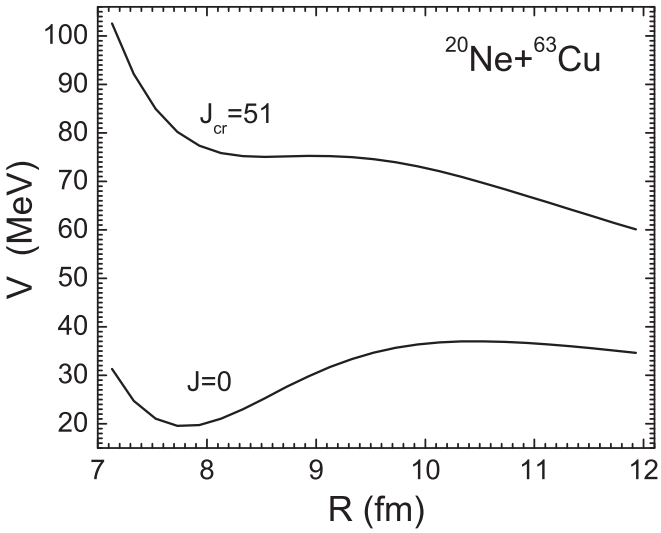

FIG. 1. The nucleus-nucleus interaction potential for the ^{20}Ne + ^{63}Cu reaction at $J = 0$ and $J = J_{cr} = 51$.

and bending modes. So, it is energetically costly to impart spin to the light fragment. In comparison, for the bending and tilting modes, the heavy fragment bears most of spin in the asymmetric DNS and for the twisting mode, both fragments carry equal spins for any DNS. Under these circumstances, the wriggling mode is ignored in our further analysis.

III. CALCULATED RESULTS AND DISCUSSIONS

A. DNS potential energy and nucleus-nucleus interaction potential

With the density-dependent effective nucleon-nucleon interaction [48,49] a repulsive core appears in V (see Figs. 1 and 2) which prevents the motion to smaller distances $(R < R_1[1 + \sqrt{5/(4\pi)}\beta_1] + R_2[1 + \sqrt{5/(4\pi)}\beta_2]$,

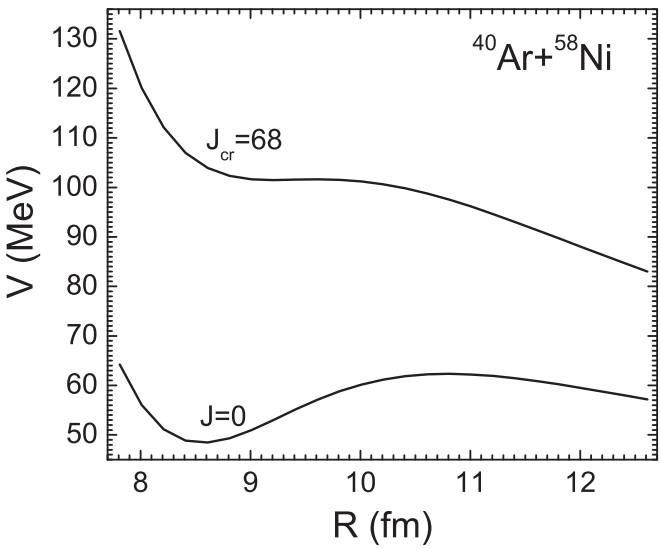

FIG. 2. The nucleus-nucleus interaction potential for the ^{40}Ar + ^{58}Ni reaction at $J = 0$ and $J = J_{cr} = 68$.

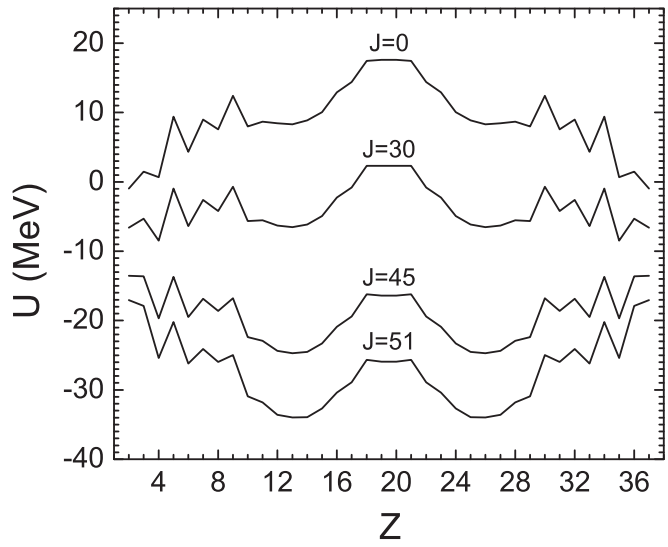

FIG. 3. The driving potential for the ^{20}Ne + ^{63}Cu system at the indicated angular momenta. The potential energy is normalized to the potential energy of the rotating CN. The total energies of the bearing modes are taken zero.

where $R_i = r_0 A_i^{1/3}$ and β_i are the radii and quadrupole deformations [50] of interacting nuclei) and reflects the action of the Pauli principle. Because of the sum of the repulsive Coulomb and centrifugal summands with attractive nuclear one, the nucleus-nucleus potential has a pocket with a minimum situated for pole-pole orientation at the touching distance $R = R_m \approx R_1(1 + \sqrt{5/(4\pi)}\beta_1) + R_2(1 + \sqrt{5/(4\pi)}\beta_2) + 0.5$ fm between the nuclei. The DNS is localized in the minimum of this pocket. At $J = 0$, the position of the Coulomb barrier in V corresponds to $R = R_b \approx R_m + 2$ fm in the DNS under consideration. Then the depth of the potential pocket is $B_R^{qf}(Z, A, J)$. The quasifission barrier B_R^{qf} prevents the DNS decay. The value of B_R^{qf} decreases with increasing J because of the growth of the repulsive centrifugal force. In the entrance channel, the potential pocket disappears at some critical value $J = J_{cr}$ (Figs. 1 and 2). So, the capture of projectile by the target is impossible at $J > J_{cr}$. The depth of the potential pocket depends also on the charge asymmetry of the DNS corresponding to given CN. For the asymmetric DNS, the interaction potential pocket is deeper than that for more symmetric configurations.

The potential energies $U(R_m, Z, A, J)$ of the DNS versus Z are presented in Figs. 3 and 4 for the systems ^{20}Ne + ^{63}Cu and ^{40}Ar + ^{58}Ni at different values of J. Note that since the isotopic composition of the nuclei forming the DNS is chosen with the condition of a N/Z equilibrium in the system [38], the mass and charge evolutions are related to each other. Because the mode responsible for the N/Z equilibrium in the DNS is the fast one, the potential energies U are minimized with respect to the mass asymmetry for each fixed charge asymmetry. It is necessary to note that the driving potential is sensitive to the total mass number of the DNS. The odd-even staggering decreases with increasing N/Z ratio in the system and the potential energy U is more flat for the neutron-rich DNS.

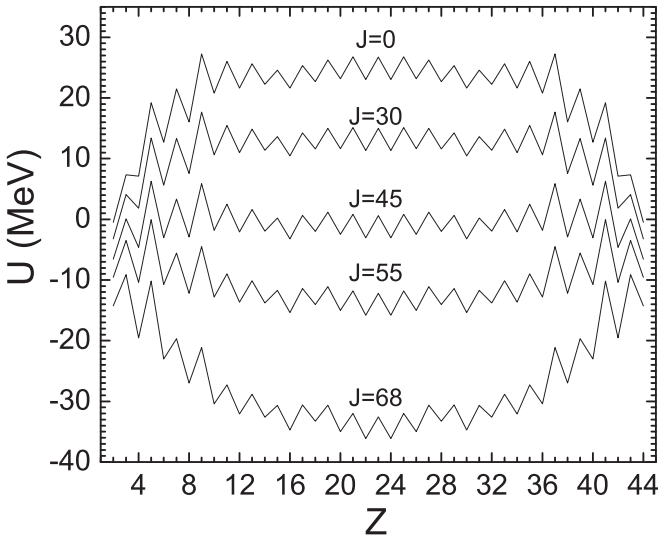

FIG. 4. The same as in Fig. 3, but for the ^{40}Ar + ^{58}Ni system.

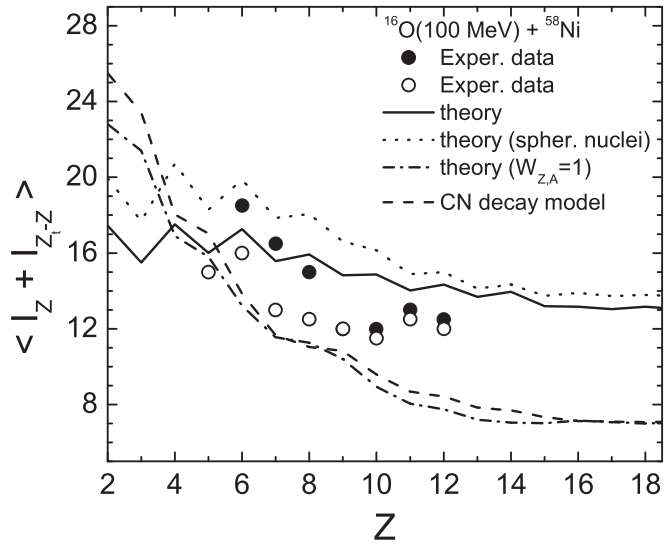

FIG. 5. The experimental (symbols) [2,15] and calculated (lines) sum of the average fragment spins vs the charge number of the light fragment in the ^{16}O (100 MeV) +^{58}Ni reaction. The experimental data are presented for the laboratory angles of 70 deg (closed circles) and 35 deg (open circles). The results calculated with and without considering the quadrupole deformations of the DNS nuclei are shown by solid and dotted lines, respectively. The results calculated with Eq. (15) (dash-dotted line) and with the CN decay model of Ref. [23] (dashed line) are presented as well.

At high angular momenta, the potential energies U of some DNS (Figs. 3 and 4), normalized to the energy of rotating CN, become negative; i.e., these configurations seems to be energetically more favorable than the CN configuration. So, the complete fusion becomes energetically hindered. Thus, at high J the quasifission contribution is larger than the complete fusion contribution to the production of binary fragments.

B. Comparisons with the experimental data

For the reactions ^{16}O ($E_{\rm lab}$ = 100 MeV) + ^{58}Ni [$E^*_{\rm CN}(J = 0) = 75$ MeV, $J_{\rm max} = J_{\rm cr} = 45$] (Fig. 5) and ^{40}Ar($E_{\rm lab}$ = 237 MeV) + ^{89}Y [$E^*_{\rm CN}(J = 0) = 122$ MeV, $J_{\rm max} = J_{\rm cr} = 78$] (Fig. 6), the sum of the average fragment spins as a function of Z is calculated by using Eq. (10). The large increase of fragment spin with charge asymmetry indicates that the DNS approaches a sticking condition [4]. In the limit, such a condition is expected to lead to a rigid rotation of the composite system in which the initial orbital angular momentum is partitioned according to the moments of inertia of the fragments and of the composite system.

As seen, the DNS model describes quite well the experimental data [4,23]. In our model, the maximum angular momentum for capture leading to fusion and quasifission reactions is always smaller than the critical angular momentum. This means that the DNS is captured in the potential pocket (because of the balance between attractive and repulsive forces) and reseparations of the DNS into two fragments occur in time larger than that required for the DNS revolution by 360 deg. Because for the reactions ^{16}O ($E_{\rm lab}$ = 100 MeV) +^{58}Ni (Fig. 5) and ^{40}Ar ($E_{\rm lab}$ = 237 MeV) +^{89}Y (Fig. 6), the experimental data [2,4,15,23] and calculated results are in rather good agreement, one can conclude that the measured data are mainly related to the fusion-fission and quasifission processes.

Note that in Ref. [4] it was concluded that the ^{40}Ar ($E_{\rm lab}$ = 237 MeV) +^{89}Y reaction fragments observed at large angle of 55 deg do result from a very narrow range of partial waves near the fusion limit. The measured anisotropic γ-ray emission indicates a strong fragment alignment and the magnitudes of average fragment spin are in very good agreement with the values calculated for rigid rotation of the DNS formed in collisions with projectile partial wave $J = 70$ near the limiting angular momentum for evaporation residue production [4]. It is sufficient to stress that the measured γ-ray multiplicities and derived angular momenta [4] are smaller at other angles (<55 deg).

It should be stressed that a relatively long reaction time is also responsible for a full relaxation of the bearing modes versus charge (mass) asymmetry.

Employing Eqs. (10) and (2), one can calculate the average γ-ray multiplicity of the two complementary fragments with atomic numbers Z and $Z_t - Z$:

$$\begin{aligned} M_\gamma &= M_\gamma(Z) + M_\gamma(Z_t - Z) \\ &= \sum_A [M_\gamma(Z,A) + M_\gamma(Z_t - Z, A_t - A)] \\ &= \tfrac{1}{2}\left[\langle I_Z^T\rangle + \langle I_{Z_t-Z}^T\rangle\right] + a_\gamma. \end{aligned} \tag{13}$$

For the reactions ^{20}Ne (166 MeV) + ^{63}Cu [$E^*_{\rm CN}(J = 0) = 125$ MeV, $J_{\rm max} = J_{\rm cr} = 51$] (Fig. 10), ^{20}Ne (175 MeV) + $^{\rm nat}$Ag [$E^*_{\rm CN}(J = 0) = 128$ MeV, $J_{\rm max} = J_{\rm cr} = 63$] (Fig. 12), ^{40}Ar (237 MeV) + ^{89}Y [$E^*_{\rm CN}(J = 0) = 122$ MeV, $J_{\rm max} = J_{\rm cr} = 78$] (Fig. 6), and ^{40}Ar (288, 340 MeV) + ^{107,109}Ag [$E^*_{\rm CN}(J = 0) = 236,288$ MeV, $J_{\rm max} = J_{\rm cr} = 97$] (Fig. 7), the calculated M_γ as a function of the charge number of one fragment are in good agreement with the experimental data. Although the parameter a_γ is adjusted for the better description of the experimental γ multiplicities, it does not influence the dependence of M_γ on Z. Besides one case in Fig. 7, $a_\gamma < 2$ in our calculations.

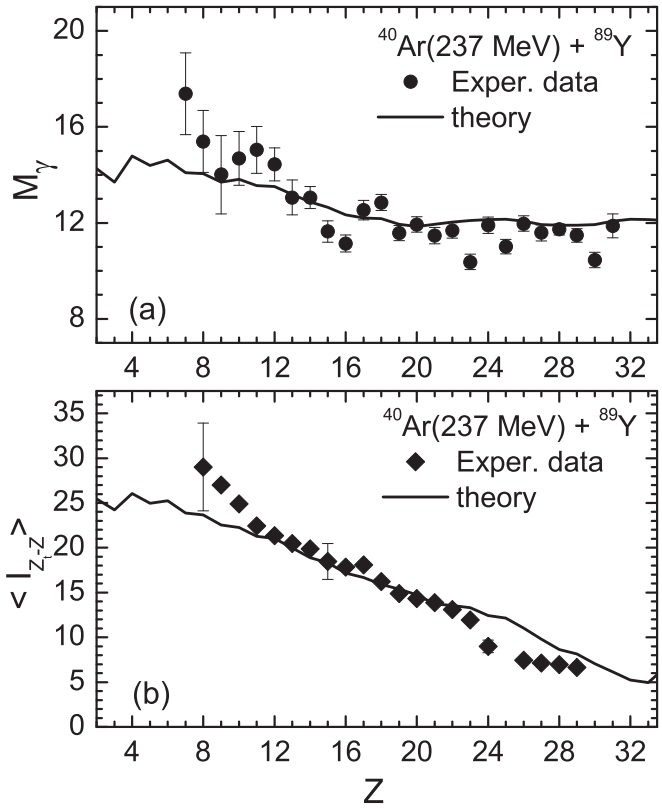

FIG. 6. The calculated (a) γ-ray multiplicity ($a_\gamma = 1.6$) and (b) average spin of the heavy fragment (solid lines) as a function of the charge number of the light fragment in the ^{40}Ar (237 MeV) +^{89}Y reaction. The experimental data (symbols) [4,23] are presented for the laboratory angle of 55 deg.

Using Eqs. (11) and (12), the widths of the fragment spin distributions in the ^{20}Ne (166 MeV) + ^{63}Cu reaction are calculated (Fig. 8). The contributions from the bending and twisting modes decrease with increasing charge asymmetry, while the contribution from the rigid rotation increases and dominates for very asymmetric DNS. For the symmetric and not strongly asymmetric fragmentations, the main process forming the width is the bending vibrations. By adding the contribution from the orbital motion to the contributions from the bearing modes, the total width remains approximately constant, which is in a good agreement with the experimental data. The calculated root mean square of the single fragment spins [Fig. 9(b)] in the ^{40}Ar (280 MeV) +^{58}Ni reaction are in fairly good agreement with the experimental data [7]. In this reaction, the maximum angular momentum is set to the critical value $J_{\max} = J_{\rm cr} = 68$ and the excitation energy of the CN ^{98}Pd is $E^*_{\rm CN}(J = 0) = 151$ MeV.

C. Role of the formation-decay probability

To emphasize the role of the formation-decay (emission) probability $W_{Z,A}(E^*_{\rm CN}, J)$, the average spins of the fragments in the ^{20}Ne (166 MeV) +^{63}Cu reaction are calculated also with Eq. (1) for two values of J: $J = J_{\rm cr}$ and $J = J_{\rm cr}/\sqrt{2}$ (Fig. 10). While this simple formula (1) describes the experimental data for the symmetric binary fragmentations, it fails to reproduce

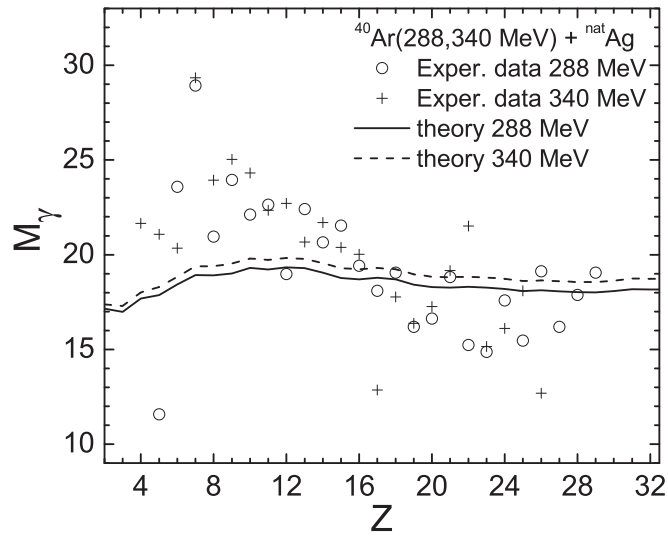

FIG. 7. The calculated γ-ray multiplicity ($a_\gamma = 5$) as a function of fragment charge number in the reactions ^{40}Ar (288 MeV) +^{107,109}Ag (solid line) and ^{40}Ar (340 MeV) +^{107,109}Ag (dashed line). The experimental data (symbols) are from Ref. [5].

the results at large asymmetries. As seen in Fig. 11, the average orbital angular momentum

$$\langle J \rangle = \frac{\sum_A \sum_{J=0}^{J_{\max}} J \sigma_{Z,A}(E_{\rm c.m.}, J)}{\sum_A \sum_{J=0}^{J_{\max}} \sigma_{Z,A}(E_{\rm c.m.}, J)} \tag{14}$$

of the DNS is nearly constant as a function of Z for almost symmetric fragmentations due to the dominance of the high partial waves and then drop off rather abruptly because of the

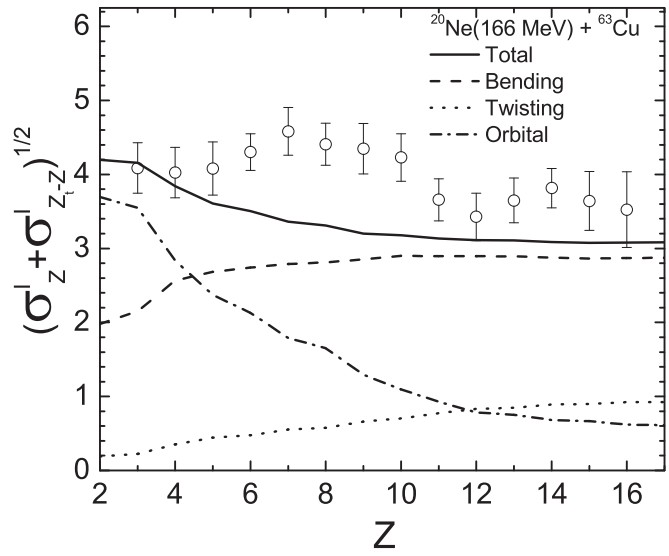

FIG. 8. The calculated square root of the sum of variances of the fragment spin distributions (solid line) vs the charge number of the light fragment in the ^{20}Ne (166 MeV) + ^{63}Cu reaction. The contributions from the orbital motion (dash-dotted line), bending (dashed line), twisting (dotted line) modes are shown. The experimental data (circles) are from Ref. [6].

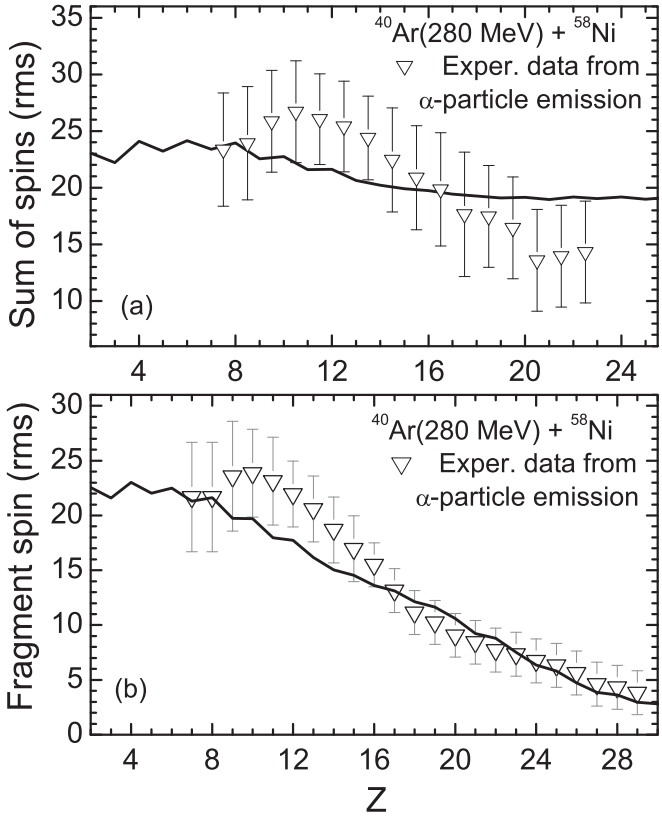

FIG. 9. The calculated (solid lines) roots mean square of the single fragment spin (b) and of the sum of fragment spins (a) as a function of the charge number of one of the fragments in the ^{40}Ar (280 MeV) +^{58}Ni reaction. The experimental data (symbols) are from Ref. [7].

small contribution of high partial waves at large asymmetries. This phenomenon is so-called the angular momentum fractionation effect [8,17]. The statistical and dynamical aspects of the angular momentum fractionation are in a good agreement with the DNS model. As seen from the driving potentials U for the reactions ^{20}Ne + ^{63}Cu (Fig. 3) and ^{40}Ar + ^{58}Ni (Fig. 4), with increasing J the driving potential starts developing a deep minimum for symmetric configurations. This minimum appears for negative values of the driving potential and the quasifission becomes energetically favorable. In the virtue of Eq. (17), which links the yield to the average spin of the fragment, the dynamical angular momentum fractionation effect is closely related to the wide spread of the low partial waves in the mass and/or charge asymmetry coordinate, while the high waves localize near symmetry. Taking into account that for a very asymmetric projectile-target pair the amount of angular momenta injected in the system is rather low, the high partial waves have an influence only at high incident energy.

To show the effect of the formation-decay probability even further, we considered the case of $W_{Z,A}(E_{\mathrm{c.m.}}, J) = 1$ (the J-independent probability) in Eq. (9); i.e., the average spin of the fragment $''i''$ ($i = 1$ or 2) arising from the orbital motion is

$$\langle I_i \rangle = \frac{\Im_i}{\Im_1 + \Im_2 + \Im_R} \frac{\sum_{J=0}^{J_{\max}} J\sigma_{\mathrm{cap}}(E_{\mathrm{c.m.}}, J)}{\sum_{J=0}^{J_{\max}} \sigma_{\mathrm{cap}}(E_{\mathrm{c.m.}}, J)}. \quad (15)$$

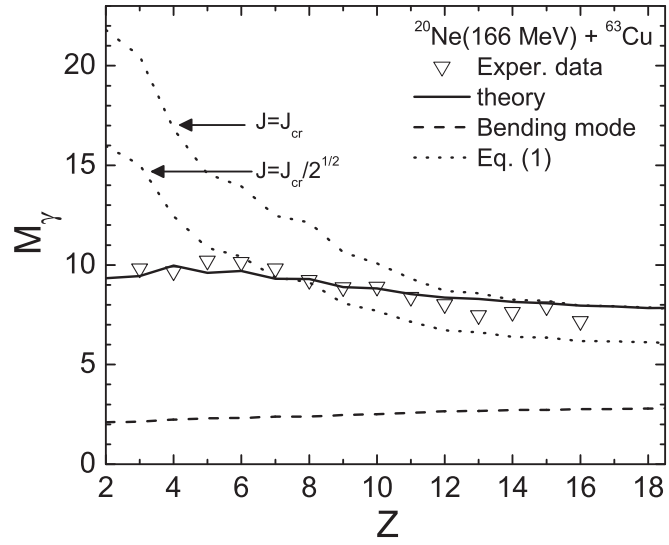

FIG. 10. The calculated (solid line) γ-ray multiplicities ($a_\gamma = 0$) deduced from the calculated sum of the fragment spins as a function of charge number of light fragment in the ^{20}Ne (166 MeV) +^{63}Cu reaction. The contribution from the bending mode is shown by a dashed line. The results of calculations with Eq. (1) and $J = J_{\mathrm{cr}}, J_{\mathrm{cr}}/\sqrt{2}$ are indicated by dotted lines. The experimental data (triangles) are from Ref. [6].

For the reactions ^{16}O (100 MeV) + ^{58}Ni and ^{20}Ne (175 MeV) + $^{\mathrm{nat}}$Ag, the important role of the redistribution of angular momenta due to the formation-decay probability becomes clear in Figs. 5 and 12. Without taking into consideration the dependence of $W_{Z,A}(E_{\mathrm{c.m.}}, J)$ on the J, Eq. (15) fails to reproduce the experimental data [15,23]. One can explain this by observing the strong dependence of the driving potential on the angular momentum (Figs. 3 and 4). As the angular momentum of the system increases, the minimum in the

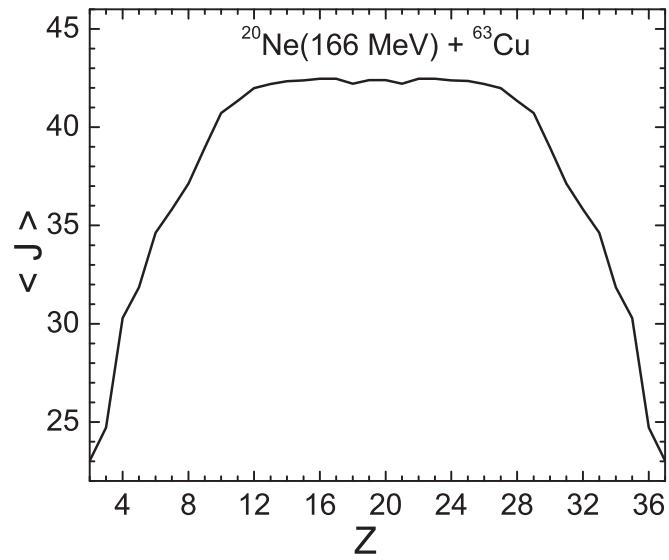

FIG. 11. The calculated average orbital angular momentum of the DNS as a function of charge number of one DNS nuclei in the ^{20}Ne (166 MeV) + ^{63}Cu reaction.

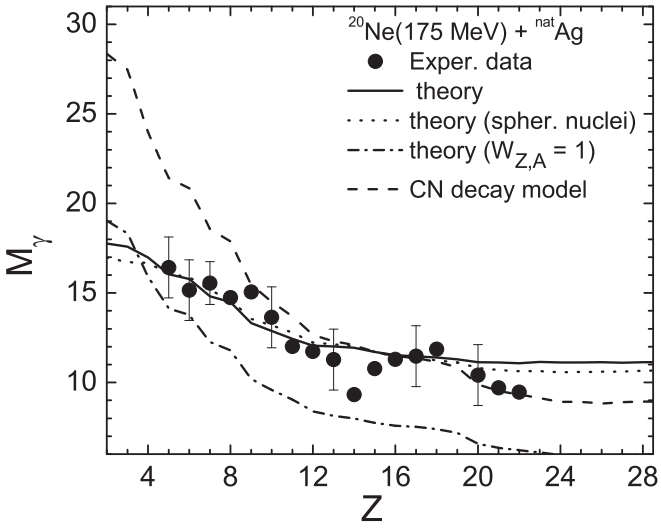

FIG. 12. The calculated sum of the average fragment spins with (solid line) and without (dotted line) considering the fragment deformations in the ^{20}Ne (175 MeV) + ^{nat}Ag reaction. The results calculated with Eq. (15) (dash-dotted line) and with the CN decay model of Ref. [23] (dashed line) are also plotted. The conversion from the γ-ray multiplicities to the fragment spins is performed with Eq. (13) and $a_\gamma = 1$. The experimental data (symbols) are from Ref. [23].

driving potential U becomes deeper and shifts to the symmetric configurations. As shown in Ref. [37], for the large angular momenta the symmetric fragmentation channels are favorable; that results in an enhanced yield near symmetry. This indicates that only low-J waves are feeding the asymmetric region far from the entrance channel. As a consequence, the mean total angular momentum is expected to decrease with increasing asymmetry. This decrease explains the deviation of results of Eq. (1) from the experimental data in Fig. 10.

For the ^{16}O (100 MeV) + ^{58}Ni reaction, the calculations with Eq. (15) and with the CN decay model of Ref. [23] give the close values of the sum of the average fragment spins (Fig. 5). In the latter model, the excitation of the bearing modes in the ^{20}Ne (175 MeV) + ^{nat}Ag reaction leads to an overestimation of the average γ-ray multiplicities M_γ from both fragments at large asymmetries (Fig. 12).

D. Role of deformations of the DNS nuclei

For comparison, we also show the results of the calculations without taking into consideration the deformations of the DNS nuclei. As clearly seen in the reactions ^{16}O (100 MeV) + ^{58}Ni (Fig. 5) and ^{20}Ne (175 MeV) + ^{nat}Ag (Fig. 12), the dependence of $\langle I_Z \rangle$ or M_γ on deformations is rather weak.

E. Role of bombarding energy in the ^{40}Ar + ^{89}Y reaction

An important quantity in heavy-ion reaction is the center-of-mass kinetic energy which governs the key aspects of collision, such as the fusion cross section, the amount of angular momenta injected into the system, excitation energies, and temperatures. Thus, it is interesting to study the evolution

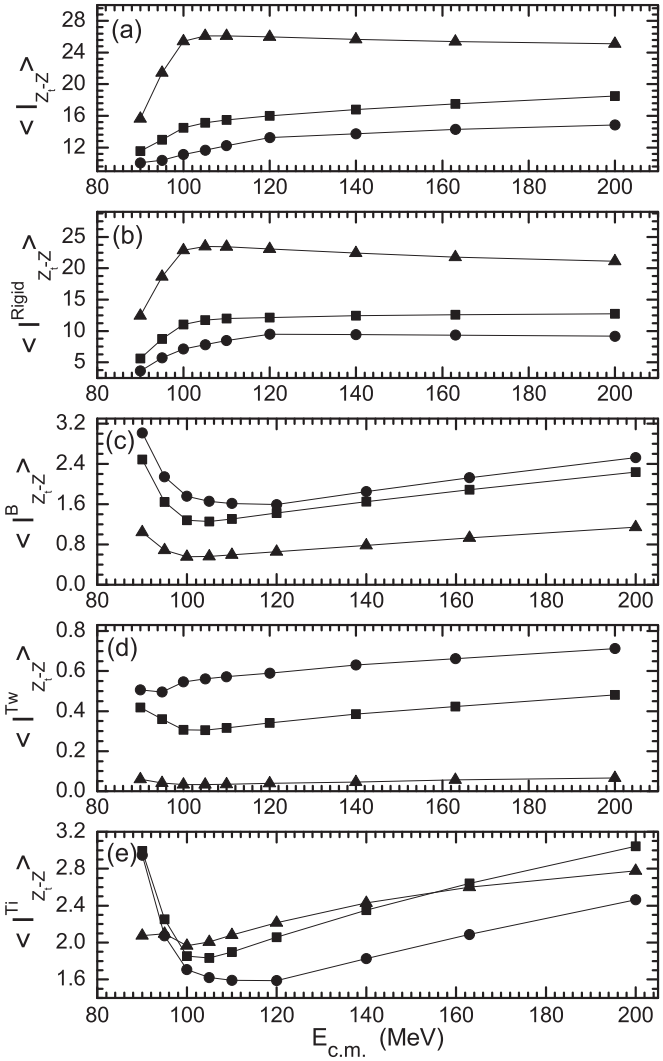

FIG. 13. The calculated average total spins $\langle I_{Z_t-Z} \rangle$ (a) and total spin components arising from the pure excitation of the orbital $[\langle I^{Rigid}_{Z_t-Z} \rangle]$ (b), bending $[\langle I^{B}_{Z_t-Z} \rangle]$ (c), twisting $[\langle I^{Tw}_{Z_t-Z} \rangle]$ (d), and tilting $[\langle I^{Ti}_{Z_t-Z} \rangle]$ (e) modes of the fragments with $Z_t - Z = 33$ (circles), 40 (squares), and 51 (triangles) as a function of $E_{c.m.}$ in the ^{40}Ar + ^{89}Y reaction.

of the spin distribution as $E_{c.m.}$ goes from low to higher values in the ^{40}Ar + ^{89}Y reaction. For the selected fragments with $Z_t - Z = 33$, 40, and 51, the evolution of the average spin with $E_{c.m.}$ is plotted in Fig. 13(a). As the value of $E_{c.m.}$ increases, the amount of angular momentum deposited into the system also increases until it reaches the critical value J_{cr}. This in turn leads to an increase of the orbital angular momentum of the final DNS available to be imparted to the final fragments, explaining the rapid increase of the spin of the fragments with energy [Fig. 13(b)]. At $E_{c.m.}$ with $J_{max} = J_{cr}$, an increase of angular momentum due to the orbital motion becomes impossible, and only the bending, twisting, and tilting modes contribute further to the fragment's spin. In fact, the spin of the fragments due to orbital motion even decreases due to the decrease of the production cross section. For the $Z_t - Z = 51$ fragment, this is clearly seen in Fig. 13(a). The saturation of

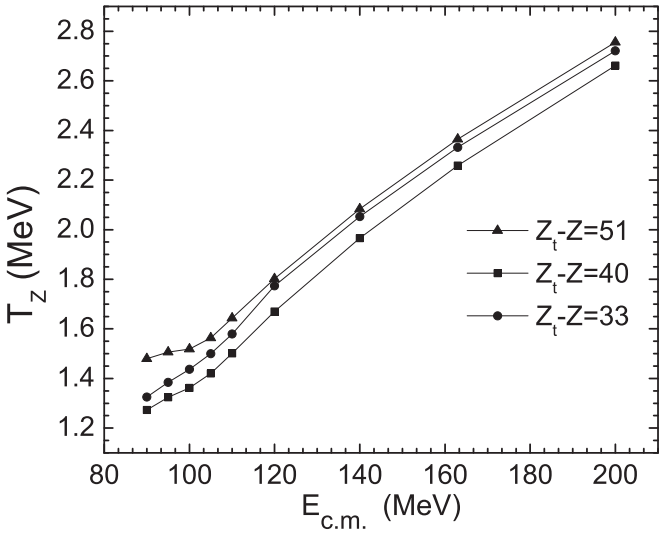

FIG. 14. The calculated average temperatures of the DNS with $Z_t - Z = 33$ (circles), 40 (squares), and 51 (triangles) as a function of the center of mass energy in the ^{40}Ar + ^{89}Y reaction.

the angular momenta of the fission fragments at high energies has been suggested in Ref. [18] and experimentally verified in the ^{40}Ar + $^{\text{nat}}$Ag reaction [5].

In Figs. 13(c)–13(e), the contributions to the heavy-fragment spin from the bending, twisting, and tilting modes are presented. Because these contributions are inversely proportional to the spin arising from the rigid rotation (see Appendix A), they generate less angular momentum as the $E_{\text{c.m.}}$ increases at $J_{\max} < J_{\text{cr}}$, even though the temperature of the system slightly increases. Once the $J_{\max}$ reaches J_{cr}, the DNS temperature

$$T_Z = \sum_{A,J=0}^{J_{\max}} \sigma_{Z,A}(E_{\text{c.m.}},J)T_{Z,A}(J)/\sum_{A}\sigma_{Z,A}(E_{\text{c.m.}})$$

rises more abruptly with $E_{\text{c.m.}}$ (Fig. 14) and the contributions of bearing modes increase. In fact, once the critical angular momentum is reached only these modes are responsible for any further increase of the spin. In Fig. 14, $\langle U(R_m, Z_t - Z = 51)\rangle < \langle U(R_m, Z_t - Z = 33)\rangle < \langle U(R_m, Z_t - Z = 40)\rangle$, where

$$\langle U(R_m,Z)\rangle = \sum_{A,J=0}^{J_{\max}} \sigma_{Z,A}(E_{\text{c.m.}},J)U(R_m,Z,A,J)\Big/\sum_{A}\sigma_{Z,A}(E_{\text{c.m.}}),$$

and, correspondingly, the configuration with $Z_t - Z = 40$ has the lowest temperature. Note that $\langle U(R_m, Z_t - Z = 51, J = 0)\rangle = 4.9$, $\langle U(R_m, Z_t - Z = 40, J = 0)\rangle = 17.4$, and $\langle U(R_m, Z_t - Z = 33, J = 0)\rangle = 13.0$ at $J = 0$ and the final averaged temperatures T_Z depend on the angular momentum fractionation effect.

In Fig. 13, one can observe that the bending and twisting modes tend to be suppressed with increasing mass (charge) asymmetry. However, they cause a weak increase in the average spin of the fragment. Note that the spin produced by the twisting mode are considerably small with respect to those from the bending and tilting modes.

IV. CONCLUSIONS

Employing the DNS model and the coupling with angular momentum bearing (bending, twisting, and tilting) modes, we have studied the characteristics of fragment spin distributions in heavy-ion collisions at energies above the Coulomb barrier. The thermal equilibrium of the collective modes of the DNS with the internal degrees of freedom has been assumed. The excitation of bearing modes causes an increase of the average fragment spin over the rigid rotational value and leads to an appreciable variation of the width of spin distributions. The effect of the bearing modes decreases with increasing asymmetry of the DNS. The spin distributions of complex fragments calculated with the DNS model agree well with the available experimental data. For strongly asymmetric decays, we have shown that one can expect a lower value of the average spin compared with other models that is in a good agreement with the experimental data. This effect is related to the small contribution of high partial waves at large charge (mass) asymmetry (angular momentum fractionation effect). For the heavy and superheavy systems, one can probably use the angular momentum fractionation effect to discriminate the fusion-fission events (with low spin) from the quasifission ones (with high spin) near the symmetry by measuring the average fragment spin.

We have also proven a connection between the entrance channel and the intrinsic rotation of the resulting fragments, dictated by the angular momentum deposited into the system. The angular momentum can be controlled either by the mass or charge asymmetry of the target-projectile system or by the incident energy of the projectile. As shown, there is a limit on the maximum amount of intrinsic spin of fragments. This limit is reached when the bombarding energy is high enough and the angular momentum of the system reaches the critical value. We hope that a new look at relatively old experimental data might trigger deeper studies of similar reactions with new facilities.

ACKNOWLEDGMENTS

This work was supported in part by DFG–RFBR (Contract No. Le439/6-1). The Romania–JINR (Dubna), IN2P3 (France)–JINR (Dubna), and Polish–JINR (Dubna) Cooperation Programmes are gratefully acknowledged. The work of N.V.A. was partly supported by a Tomsk Polytechnic University Competitiveness Enhancement Program grant.

APPENDIX

For the sake of completeness, we present here the most important features of the bearing modes from Ref. [9]. Let us treat the DNS in the body-fixed system in which the disintegration (symmetry) axis is the y axis. The total angular momentum of the system $\mathbf{I}$ is equal to the initial orbital angular momentum $\mathbf{J}$ in the entrance channel. When the DNS decays, $\mathbf{I}$ is imparted to the intrinsic spin $\mathbf{S_i}$ of the fragments and to the orbital angular momentum $\mathbf{l}$: $\mathbf{I} = \mathbf{S_1} + \mathbf{S_2} + \mathbf{l}$. The projection of $\mathbf{I}$ on the disintegration axis is K. The total rotational energy

of the system is

$$V_R = \frac{S_1^2}{2\Im_1} + \frac{S_2^2}{2\Im_2} + \frac{l^2}{2\Im_R}.$$

Here, $\hbar = 1$ for the simplicity and the index $i = 1$ refers to the DNS heavy fragment. The spin components of this fragment "1" are

$$S_{1x} = \frac{\Im_1}{\Im}\sqrt{I^2 - K^2}\sin(\Omega t) + R_{1x} = I_{R_1}\sin(\Omega t) + R_{1x},$$

$$S_{1y} = \frac{\Im_1}{\Im_1 + \Im_2}K + R_{1y},$$

$$S_{1z} = I_{R_1}\cos(\Omega t) + R_{1z}.$$

The first terms in the expressions above originate from the rigid rotation of the system and the second terms arise from the excitation of the collective modes. Imposing the angular momentum conservation, one obtains the following constraints:

$$I_x = l_x + R_{1x} + R_{2x} + (I_{R_1} + I_{R_2})\sin(\Omega t),$$

$$I_y = K = R_{1y} + R_{2y} + K,$$

$$I_z = l_z + R_{1z} + R_{2z} + (I_{R_1} + I_{R_2})\cos(\Omega t).$$

One immediately observes that $R_{1y} = -R_{2y}$. The quadratic form of $V_{bm} = V_R - I^2/2\Im$ is written after diagonalization

$$V_{bm} = \frac{1}{2}\left(\epsilon_{Wx}^2 + \epsilon_{Bx}^2 + \epsilon_{Ti}^2 + \epsilon_{Tw}^2 + \epsilon_{Wz}^2 + \epsilon_{Bz}^2\right),$$

where the normal coordinates $\epsilon_{Ti} = K\sqrt{\frac{\Im_R}{\Im(\Im_1+\Im_2)}}$, $\epsilon_{Tw} = R_y\sqrt{\frac{\Im_1+\Im_2}{\Im_1\Im_2}}$, $\epsilon_{Wx} = R_{1x}/a_{1Wx}$, $\epsilon_{Wz} = R_{1z}/a_{1Wz}$, and $\epsilon_{Bx} = R_{1x}/a_{1Bx}$, $\epsilon_{Bz} = R_{1z}/a_{1Bz}$ of the tilting, twisting, wriggling, and bending modes, respectively. The fragment spin components of the eigenvectors are

$$\begin{aligned} a_{1Ti} &= \Im_1\sqrt{\frac{\Im}{\Im_R(\Im_1+\Im_2)}}, \\ a_{2Ti} &= \Im_2\sqrt{\frac{\Im}{\Im_R(\Im_1+\Im_2)}}, \end{aligned} \tag{A1}$$

for the tilting mode,

$$a_{1Tw} = -a_{2Tw} = \sqrt{\frac{\Im_1\Im_2}{\Im_1+\Im_2}}$$

for the twisting mode, and

$$\begin{aligned} a_{1B} &= -a_{1W} = -\Im_1\left[\frac{\Im_2}{\Im_1^2\Im_R(\Im_2+\Im_R)\lambda_B^2 + (\Im_1+\Im_R-2\Im_1\Im_R\lambda_B)\Im}\right]^{1/2}, \\ a_{2B} &= a_{2W} = \Im_2\left[\frac{\Im_1}{\Im_2^2\Im_R(\Im_1+\Im_R)\lambda_B^2 + (\Im_2+\Im_R-2\Im_2\Im_R\lambda_B)\Im}\right]^{1/2}, \\ \lambda_B &= \frac{1}{2}\left[\frac{1}{\Im_1}+\frac{1}{\Im_2}+\frac{2}{\Im_R} \mp \sqrt{\left(\frac{1}{\Im_1}+\frac{1}{\Im_2}\right)+\left(\frac{2}{\Im_R}\right)^2}\right] \end{aligned} \tag{A2}$$

for the bending ($a_{1B,2B}$ and λ_B with a minus sign) and wriggling ($a_{1W,2W}$ and λ_B with a plus sign) modes.

Let us now calculate the various moments of the fragment spin distributions for the normal modes. Because of the double degeneracy, the bending mode produces angular momenta orientated randomly in the xz plane. The excitation of this mode will produce the spin components R_{1x} and R_{1z}. With new variables $\zeta^2 = \epsilon_{Bx}^2 + \epsilon_{Bz}^2$ and $\theta = \tan^{-1}(\epsilon_{Bx}/\epsilon_{Bz})$, the total spin of the fragment "1" is $S_1 = \sqrt{R_1^2 + I_{R_1}^2 + 2R_1 I_{R_1}\cos\theta}$, where $R_1^2 = R_{1x}^2 + R_{1z}^2$. The partition function is $Z = 2\pi\tau$ and, thus, the average spin is

$$\begin{aligned} \left\langle S_1^B\right\rangle \approx I_{R_1} &+ \frac{a_{1B}^2\tau}{2I_{R_1}} - \frac{1}{2}\left(\frac{a_{1B}^2\tau}{I_{R_1}} + \frac{I_{R_1}}{2}\right)\exp\left(-\frac{I_{R_1}^2}{2a_{1B}^2\tau}\right) \\ &+ \sqrt{2\pi\tau}\left(\frac{a_{1B}}{2} + \frac{I_{R_1}^2}{8\tau a_{1B}}\right)\mathrm{erfc}\left(\frac{I_{R_1}}{a_{1B}\sqrt{2\tau}}\right). \end{aligned} \tag{A3}$$

Here, $\tau = T_{Z,A}$ is the temperature of the given DNS. The similar derivation of the second moment for the fragment "1" gives $\langle (S_1^B)^2\rangle = I_{R_1}^2 + 2a_{1B}^2\tau$. Employing the above equations, one can calculate the variance σ_1^B of the spin distribution for the fragment "1." For large I_{R_1}, $\sigma_1^B \simeq a_{1B}^2\tau$.

For the γ-ray multiplicity measurements which are not sensitive to the spin distributions of the individual fragments, one should consider the total spin of fragments, $S^B = |S_1^B| + |S_2^B|$. The width of the spin distribution due to the bending mode is calculated as

$$\sigma^B = \left\langle \left(\left|S_1^B\right| + \left|S_2^B\right|\right)^2\right\rangle - \left\langle \left|S_1^B\right| + \left|S_2^B\right|\right\rangle^2 \approx (|a_{1B}| + a_{2B})^2\tau.$$

The spin of the fragment "1" due to the twisting mode is

$$\begin{aligned} \left\langle S_1^{Tw}\right\rangle \approx &\left(I_{R_1} + \frac{a_{1Tw}^2\tau}{2I_{R_1}}\right)\mathrm{erf}\left(\frac{I_{R_1}}{a_{1Tw}\sqrt{2\tau}}\right) \\ &+ \frac{a_{1Tw}}{2}\sqrt{\frac{2\tau}{\pi}}e^{-I_{R_1}^2/2a_{1Tw}^2\tau} \\ &+ \frac{I_{R_1}^2}{2a_{1Tw}\sqrt{2\pi\tau}}E_1\left(\frac{I_{R_1}^2}{2a_{1Tw}^2\tau}\right), \end{aligned} \tag{A4}$$

where $E_1(x) = \int_x^\infty dt e^{-t} t^{-1}$ is the exponential integral. The calculation of $\langle (S_1^{Tw})^2 \rangle$ is easier and leads to the simple result $\langle (S_1^{Tw})^2 \rangle = I_{R_1}^2 + a_{1Tw}^2 \tau$. For small I_{R_1}, the expression for the variance arising from the twisting mode is [9]

$$\sigma_1^{Tw} = a_{1Tw}^2 \left(1 - \frac{2}{\pi}\right)\tau. \tag{A5}$$

In the limit of large I_{R_1}, $\sigma_1^{Tw} \simeq 0$. For fairly asymmetric systems, large spin limit is attained by the heavy fragment "1" and, thus, the total fluctuations due to the twisting mode come from the light fragment "2" only: $\sigma^{Tw} \simeq \sigma_2^{Tw}$.

The spin of the fragment "1" due to the tilting mode is

$$\langle S_1^{Ti} \rangle \approx I_{R_1} + \frac{1}{2I_{R_1}} \left[a_{1Ti}^2 - \left(\frac{\Im_1}{\Im}\right)^2 (a_{1Ti} + a_{2Ti})^2 \right] \langle \epsilon_{Ti}^2 \rangle,$$
$$\langle \epsilon_{Ti}^2 \rangle = \tau \left[1 - \sqrt{\frac{2}{\pi\tau}} \frac{x e^{-x^2/2\tau}}{\mathrm{erf}\left(\frac{x}{\sqrt{2\tau}}\right)} \right], \tag{A6}$$

where $x = I/(a_{1Ti} + a_{2Ti}) = I\sqrt{\frac{\Im_R}{\Im(\Im_1+\Im_2)}}$. For large I_{R_1}, $\langle \epsilon_{Ti}^2 \rangle \approx \tau$. Averaging the square of S_1^{Ti}, one obtains

$$\left\langle \left(S_1^{Ti}\right)^2 \right\rangle \approx I_{R_1}^2 + \left[a_{1Ti}^2 - \left(\frac{\Im_1}{\Im}\right)^2 (a_{1Ti} + a_{2Ti})^2 \right] \langle \epsilon_{Ti}^2 \rangle. \tag{A7}$$

For almost symmetric DNS, the fluctuations to the spin produced by the tilting mode are very small [9].

Equations (A3), (A4), and (A6) can be written as $\langle S_1^B \rangle = I_{R_1} + I_1^B$, $\langle S_1^{Tw} \rangle = I_{R_1} + I_1^{Tw}$, and $\langle S_1^{Ti} \rangle = I_{R_1} + I_1^{Ti}$, where the first term $I_1^{\mathrm{Rigid}} = I_{R_1}$ arises from the pure rigid rotation and the second term is produced by the pure excitation of the bending (I_1^B) or twisting (I_1^{Tw}), or tilting (I_1^{Ti}) modes, respectively.

[1] J. B. Wilhelmy, E. Cheifetz, R. C. Jared, S. G. Tompson, H. R. Bowman, and J. O. Rasmussen, Phys. Rev. C **5**, 2041 (1972).
[2] R. Albrecht, W. Dünnweber, G. Graw, H. Ho, S. G. Steadman, and J. P. Wurm, Phys. Rev. Lett. **34**, 1400 (1975).
[3] P. Glässel, R. S. Simon, R. M. Diamond, R. C. Jared, I. Y. Lee, L. G. Moretto, J. O. Newton, R. Schmitt, and F. S. Stephens, Phys. Rev. Lett. **38**, 331 (1977).
[4] M. N. Namboodiri, J. B. Natowitz, P. Kasiraj, R. Eggers, L. Adler, P. Gonthier, C. Cerruti, and S. Simon, Phys. Rev. C **20**, 982 (1979).
[5] L. G. Moretto, LBL-9130; CONF-790751-1; CONF-790751-2.
[6] R. A. Dayras, R. G. Stokstad, D. C. Hensley, M. L. Halbert, D. G. Sarantites, L. Westerberg, and J. H. Barker, Phys. Rev. C **22**, 1485 (1980).
[7] R. Babinet, B. Cauvin, J. Girard, J. M. Alexander, T. H. Chiang, J. Galin, B. Gatty, D. Guerreau, and X. Tarrago, Z. Phys. A **295**, 153 (1980).
[8] L. G. Moretto and R. P. Schmitt, Phys. Rev. C **21**, 204 (1980).
[9] R. P. Schmitt and A. J. Pacheco, Nucl. Phys. A **379**, 313 (1982).
[10] R. Bock *et al.*, Nucl. Phys. A **388**, 334 (1982).
[11] F. A. Dilmanian, L. Grodzins, J. W. Ball, M. Beckerman, R. Boisseau, S. Gazes, R. Ledoux, and A. Sperduto, Phys. Lett. B **127**, 172 (1983).
[12] R. P. Schmitt, G. Mouchaty, D. R. Haenni, and P. Bogucki, Phys. Lett. B **127**, 327 (1983).
[13] B. B. Back, R. R. Betts, K. Cassidy, B. G. Glagola, J. E. Gindler, L. E. Glendenin, and B. D. Wilkins, Phys. Rev. Lett. **50**, 818 (1983); B. B. Back, R. R. Betts, J. E. Gindler, B. D. Wilkins, S. Saini, M. B. Tsang, C. K. Gelbke, W. G. Lynch, M. A. McMahan, and P. A. Baisden, Phys. Rev. C **32**, 195 (1985); **33**, 385 (1985).
[14] S. Ayik, G. Wolschin, and W. Norenberg, Z. Phys. A **286**, 271 (1978); J. Q. Li and G. Wolschin, Phys. Rev. C **27**, 590 (1983).
[15] W. Dünnweber, in *Nuclear Structure and Heavy-Ion Dynamics* (North-Holland Physics Publishing, Amsterdam, 1984), p. 389.
[16] R. P. Schmitt, G. Mouchaty, and D. R. Haenni, Nucl. Phys. A **427**, 614 (1984).
[17] L. G. Moretto and G. J. Wozniak, Annu. Rev. Nucl. Part. Sci. **34**, 189 (1984); Prog. Part. Nucl. Phys. **21**, 401 (1988).
[18] D. Shapira, D. Schull, J. L. C. Ford, B. Shivakumar, R. L. Parks, R. A. Cecil, and S. T. Thornton, Phys. Rev. Lett. **53**, 1634 (1984).
[19] R. P. Schmitt, G. Mouchaty, D. R. Haenni, and M. Tirion, Z. Phys. A **321**, 411 (1985).
[20] J. Töke *et al.*, Nucl. Phys. A **440**, 327 (1985).
[21] T. Dossing and J. Randrup, Nucl. Phys. A **433**, 215 (1985); **433**, 280 (1985).
[22] K. Lützenkirchen, J. V. Kratz, G. Wirth, W. Brüchle, K. Sümmerer, R. Lucas, J. Poitou, and C. Gregoire, Nucl. Phys. A **452**, 351 (1986).
[23] L. G. Moretto, G. F. Peaslee, and G. J. Wozniak, Nucl. Phys. A **502**, 453c (1989).
[24] W. U. Schröder and J. R. Huizenga, Nucl. Phys. A **502**, 473c (1989).
[25] B. B. Back, S. Bjørnholm, T. Døssing, W. Q. Shen, K. D. Hildenbrand, A. Gobbi, and S. P. Sørensen, Phys. Rev. C **41**, 1495 (1990).
[26] Y. El Masri *et al.*, Nucl. Phys. A **517**, 340 (1990).
[27] R. K. Choudhury *et al.*, Nucl. Phys. A **654**, 845c (1999).
[28] G. G. Chubarian, M. G. Itkis, N. A. Kondratiev, E. M. Kozulin, V. V. Pashkevich, I. V. Pokrovsky, A. Ya. Rusanov, V. S. Salamatin, and R. P. Schmitt, Phys. Rev. Lett. **87**, 052701 (2001); A. Ya. Rusanov, M. G. Itkis, N. A. Kondratiev, V. V. Pashkevich, I. V. Pokrovsky, V. S. Salamatin, and G. G. Chubarian, Phys. At. Nucl. **71**, 956 (2008).
[29] G. N. Kniajeva *et al.*, Nucl. Phys. A **734**, E25 (2004).
[30] H. Naik, S. P. Dange, and R. J. Singh, Phys. Rev. C **71**, 014304 (2005).
[31] E. Vardaci *et al.*, Eur. Phys. J. A **43**, 127 (2010).
[32] Sh. A. Kalandarov, G. G. Adamian, N. V. Antonenko, and W. Scheid, Phys. Rev. C **83**, 054611 (2011).
[33] Sh. A. Kalandarov, D. Lacroix, G. G. Adamian, N. V. Antonenko, J. P. Wieleczko, S. Pirrone, and G. Politi, Phys. Rev. C **93**, 024613 (2016).
[34] J. Galin *et al.*, Phys. Rev. C **9**, 1126 (1974).
[35] L. G. Sobotka, D. G. Sarantites, Z. Li, E. L. Dines, M. L. Halbert, D. C. Hensley, J. C. Lisle, R. P. Schmitt, Z. Majka, G. Nebbia,

H. C. Griffin, and A. J. Sierk, Phys. Rev. C **36**, 2713 (1987); L. G. Sobotka (private communication).
[36] Sh. A. Kalandarov, G. G. Adamian, N. V. Antonenko, and W. Scheid, Phys. Rev. C **82**, 044603 (2010).
[37] S. A. Kalandarov, G. G. Adamian, N. V. Antonenko, W. Scheid, and J. P. Wieleczko, Phys. Rev. C **84**, 064601 (2011).
[38] V. V. Volkov, Izv. AN SSSR Ser. Fiz. **50**, 1879 (1986); G. G. Adamian, A. K. Nasirov, N. V. Antonenko, and R. V. Jolos, Phys. Part. Nucl. **25**, 583 (1994); G. G. Adamian, N. V. Antonenko, and W. Scheid, Nucl. Phys. A **618**, 176 (1997); G. G. Adamian, N. V. Antonenko, W. Scheid, and V. V. Volkov, *ibid.* **627**, 361 (1997); **633**, 409 (1998); G. G. Adamian, N. V. Antonenko, and W. Scheid, Phys. Rev. C **68**, 034601 (2003).
[39] J. G. del Campo, C. Baktash, H. Q. Jin, D. Rudolph, A. D'Onofrio, F. Terrasi, G. de Angelis, M. De Poli, C. Fahlander, A. Gadea, *et al.*, Phys. Rev. C **57**, R457(R) (1998).
[40] M. La Commara *et al.*, Nucl. Phys. A **669**, 43 (2000).
[41] J. Töke, J. Lu, and W.-U. Schröder, Phys. Rev. C **67**, 034609 (2003); B. Djerroud, D. K. Agnihotri, S. P. Baldwin, W. Skulski, J. Tõke, W. U. Schröder, R. J. Charity, J. F. Dempsey, D. G. Sarantites, L. G. Sobotka, B. Lott, W. Loveland, and K. Aleklett, *ibid.* **64**, 034603 (2001); J. Töke, D. K. Agnihotri, W. Skulski, and W.-U. Schröder, *ibid.* **63**, 024604 (2001).
[42] G. Ademard, J. P. Wieleczko *et al.*, Phys. Rev. C **83**, 054619 (2011).
[43] S. Pirrone *et al.*, J. Phys.: Conf. Ser. **515**, 012018 (2014).
[44] R. J. Charity *et al.*, Nucl. Phys. A **483**, 371 (1988).
[45] R. J. Charity *et al.*, Nucl. Phys. A **476**, 516 (1988).
[46] V. V. Sargsyan, G. G. Adamian, N. V. Antonenko, and W. Scheid, Eur. Phys. J. A **45**, 125 (2010); V. V. Sargsyan, G. G. Adamian, N. V. Antonenko, W. Scheid, and H. Q. Zhang, *ibid.* **47**, 38 (2011).
[47] A. V. Ignatyuk, *Statistical Properties of Excited Atomic Nuclei* (Energoizdat, Moscow, 1983).
[48] G. G. Adamian, N. V. Antonenko, R. V. Jolos, S. P. Ivanova, and O. I. Melnikova, Int. J. Mod. Phys. E **5**, 191 (1996).
[49] A. B. Migdal, *Theory of Finite Fermi System and Properties of Atomic Nuclei* (Nauka, Moscow, 1983).
[50] S. Raman, C. W. Nestor Jr., and P. Tikkanen, At. Data Nucl. Data Tables **78**, 1 (2001).